Latypova, Renata; Fangnon, Agbemon; Nousiainen, Olli; Pallaspuro, Sakari; Kömi, Jukka

Role of prior austenite grain structure in hydrogen diffusion, trapping, and embrittlement mechanisms in as-quenched martensitic steels

Published in:
International Conference on Structural Integrity 2023 (ICSI 2023)

DOI:
10.1016/j.prostr.2024.01.067

Published: 01/01/2024

Document Version
Publisher's PDF, also known as Version of record

Available online at www.sciencedirect.com

ScienceDirect

Procedia Structural Integrity 54 (2024) 149–155

Structural Integrity Procedia

www.elsevier.com/locate/procedia

International Conference on Structural Integrity 2023 (ICSI 2023)

Role of prior austenite grain structure in hydrogen diffusion, trapping, and embrittlement mechanisms in as-quenched martensitic steels

Renata Latypova[a,*], Eric Fangnon[b], Olli Nousiainen[a], Sakari Pallaspuro[a], Jukka Kömi[a]

[a]*University of Oulu, Materials and Mechanical Engineering, Centre for Advanced Steels Research (CASR), P.O. Box 4200, 90014 Oulu, Finland*
[b]*Aalto University School of Engineering, Department of Mechanical Engineering, P.O. Box 14200, FI-00076 AALTO, Finland*

Abstract

Prior austenite grain structure (PAG) is an essential factor in martensitic steels that affects hydrogen (H) diffusion, trapping, and susceptibility to hydrogen embrittlement (HE). The influence of PAG morphology on HE susceptibility of ultrahigh-strength steels has been previously studied with a novel tuning-fork test (TFT). To achieve different PAG morphologies with the same alloying composition, a direct-quenched steel (DQ) was reaustenitized at 860 °C (A860) and 960 °C (A960) for 25 min, followed by quenching. DQ and A860 have different PAG morphologies, elongated vs. equiaxed, but similar ~10 µm average PAG size. A860 and A960 have the same equiaxed morphology but a fourfold difference in PAG size. To evaluate the TFT method, and to provide a further understanding of the effect of PAG structure on H diffusion and trapping, in-situ constant load tensile tests (CLT), electrochemical hydrogen permeation (EP), and thermal desorption spectroscopy (TDS) measurements were conducted with the same materials. CLT produced the same results as TFT, where the original DQ material with elongated PAG structure has the best resistance against HE with the longest time-to-fracture and a quasi-cleavage crack propagation mechanism. A860 and A960 with equiaxed PAG structures are more susceptible to HE, showing partly intergranular crack propagation, linking to the geometrical shape of the PAG structure. The diffusion of H is here dominated by the simultaneous effects of the PAG surface area and dislocation density. Therefore, H diffusion is the slowest for DQ with a slight increase for A860 and A960.

Keywords: electrochemical hydrogen permeation; hydrogen embrittlement; martensite; PAG structure; TDS

* Corresponding author.
E-mail address: renata.latypova@oulu.fi

10.1016/j.prostr.2024.01.067

1. Introduction

Hydrogen embrittlement (HE) is a major concern when it comes to materials selection for the hydrogen infrastructure. To utilize hydrogen as an energy source, a safe infrastructure is required to prevent HE failures, which are caused by the combination of sufficient concentration of atomic hydrogen (H) and tensile stress. One of the prospective materials for H applications is ultrahigh-strength steels, but they require further microstructural optimization and experimental verification of the resistance against HE. HE susceptibility can be evaluated with mechanical testing, which typically combines the application of tensile stress with electrochemical/gaseous H-charging, e.g., constant load tests (CLT), slow strain rate tests (SSRT), incremental step loading tests (ISLT), and 3 or 4-point bending tests. Other techniques are used for H detection and visualization such as hydrogen permeation technique (EP) and thermal desorption spectroscopy (TDS) (Rudomilova et al., 2018).

A novel testing method called the Tuning-Fork Test (TFT) has been recently developed to specifically study the HE susceptibility of ultrahigh-strength steels (Latypova, 2022). TFT utilizes tuning-fork-shaped notched specimens, which are stressed with a loadcell clamping system using constant displacement, and then electrochemically charged with H until fracture. The integrated loadcell monitors load values, which can be correlated to crack initiation, crack propagation, and the final fracture of the specimen. TFT is a versatile test that can be operated using ISLT to determine the threshold stress level of different ultrahigh-strength steels (Latypova et al., 2023a). Constant displacement tests with elastic or plastic straining can also be conducted with TFT as simple fracture tests. In addition, the crack initiation can be studied with interrupted tests, where the specimen is taken out of the cell as soon as the crack has been initiated for precise studies of the crack tip.

TFT has been previously utilized in ranking various ultrahigh-strength steels according to HE susceptibility (Latypova, 2022). Further investigations were conducted to study the influence of prior austenite grain (PAG) size and morphology in HE-initiated failures with 500 HBW martensitic steels. The materials were tested in different H-charging environments using elastic loading of 1000 MPa as well as plastic loading producing similar results (Latypova et al., 2022, 2023b). Elongated PAG structure of the same alloy had better HE resistance with a slower crack propagation rate and quasi-cleavage cracking mechanism in comparison to equiaxed PAG structures with partly intergranular crack propagation. In this study, we aim to evaluate the novel TFT by conducting in-situ CLT with the same materials used in the PAG study. Additional TDS and EP experiments are conducted to further explain the effect of PAG structure on H diffusion and trapping mechanisms.

2. Materials and methods

Three materials were tested: a direct-quenched steel (DQ), and the same austenitized at 860 °C (A860) and 960 °C (A960) for 25 min, followed by quenching (Latypova et al., 2022, 2023b). DQ and A860 have different PAG morphologies, elongated vs. equiaxed, but similar 10 μm average PAG size. A960 has a fourfold PAG size compared to A860 but the same equiaxed PAG morphology as presented in Figure 1. All materials have an auto-tempered lath-martensitic microstructure with the same alloying composition (0.25C-0.1Si-0.25Mn wt.%) and similar mechanical properties such as tensile strength and hardness (Latypova et al., 2022, 2023b).

The surface and centerline of the steel plates were analyzed with XRD to estimate the retained austenite content (< 1%) and dislocation density of materials (Table 1). At the surface, the dislocation density is lowest for DQ, and it increases with austenitization temperature. At the centerline, DQ has the same dislocation density, and reaustenitized steels have higher dislocation density in comparison to the surface, which is most likely a consequence of the quenching of the plates.

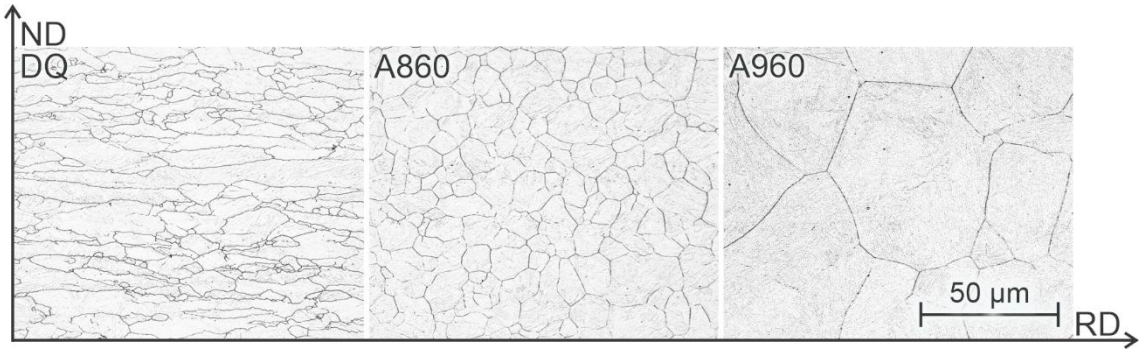

Figure 1. PAG structure of investigated materials.

Table 1. Evaluated dislocation densities of martensite using the modified Williamson-Hall method (mWH) (Ungár et al., 1998).

Steel	Surface (m^{-2})	Centerline (m^{-2})
DQ	2.60×10^{-15}	2.60×10^{-15}
A860	2.67×10^{-15}	3.66×10^{-15}
A960	3.66×10^{-15}	4.19×10^{-15}

CLT were performed with notched tensile specimens under continuous H-charging (3% NaCl + 0.3 % NH_4SCN, -1.2V_{SCE}) to determine time-to-fracture under variable load levels. Specimens were pre-charged with H for 2 h before loading. The applied loads for the respective steels were selected in the regime below the ultimate tensile strength earlier determined with SSRT under the same H-charging conditions. After the CLT, one side of the cut gauge section was used to measure H concentrations using TDS with a heating rate of 10 K/min, and the other side for fracture surface analysis with a Zeiss Sigma field-emission scanning electron microscope (FESEM). The total H concentration, diffusible H concentration (≤ 550 K), and trapped H concentration (> 550 K) were calculated from each sample by integrating the area below the temperature-desorption rate curve.

EP tests were conducted with an in-house PVC Devanathan-Stachurski cell using 0.7±0.02 mm thick specimens under the same H-charging conditions as in CLT to assess H diffusion properties (Latypova, 2023). For A860 and A960 steels, both surface and centerline regions were investigated due to variations in dislocation density, but DQ specimens were prepared only from the surface of the plate. Before H-charging, the detection side of the specimen was electroplated with 1 µm palladium coating and polarized at 0.3$V_{Hg/HgO}$ using 0.1M NaOH electrolyte until the current density dropped below 0.1 µA/cm^2. From the permeation curves, effective H diffusion coefficients (D_{eff} = D) were calculated using the breakthrough time technique (Equation 1), where L = specimen thickness and t_b = breakthrough time (ASTM G148 – 97, 2003).

$$D_{eff} = \frac{L^2}{15.3 t_b} \tag{1}$$

3. Results and discussion

Time-to-fracture results show that DQ steel has better HE resistance in comparison to A860 and A960 steels that fracture significantly faster under similar loading (Figure 2a, b), which is consistent with the previously published TFT results (Latypova et al., 2022, 2023b). However, the results for the reaustenitized steels vary with both CLT and TFT. For CLT with 400 – 600 MPa, A860 has better performance than A960 with over twofold differences in time-to-fracture results. However, the difference between A860 and A960 diminishes towards higher stress levels (Figure 2c).

At 800 MPa load, both reaustenitized steels fail extremely fast with time-to-fracture values lower-bounding to < 3 minutes and the marginal differences at 800 MPa load level are most likely caused by natural scatter.

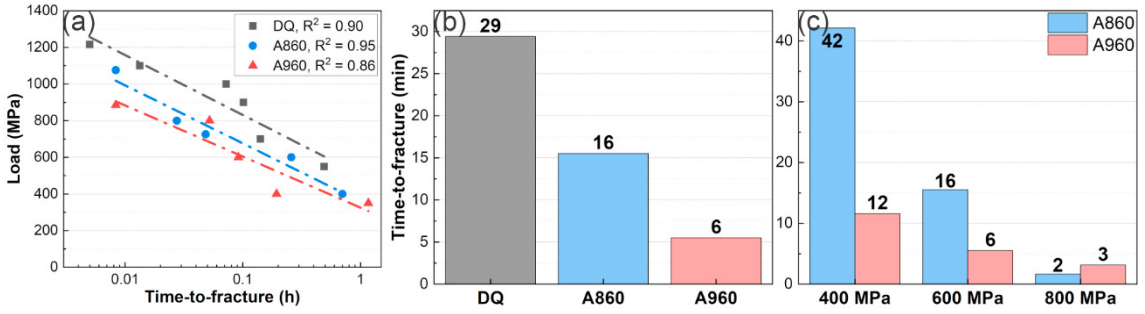

Figure 2. (a) Time-to-fracture vs. applied load of all tests, (b) comparison of all materials with 550 – 600 MPa loading and (c) time-to-fracture of A860 and A960 with 400 – 800 MPa loading.

With TFT, elastic loading of 1000 MPa and H-charging in 0.1 M H_2SO_4 + 1g/l thiourea under cathodic 1.2 $V_{Hg/HgSO_4}$ potential shows faster fracture for A860 in comparison to A960 (Latypova et al., 2023b). On the other hand, with plastic straining in the same H-charging environment as the conducted CLT, the results for A860 and A960 are the same (Latypova et al., 2023b). According to the literature, the effect of PAG size on HE susceptibility is still a controversial topic because other influencing factors arise simultaneously with the efforts to vary PAG size, such as undissolved carbides, solute elements, and retained austenite (Kimura et al., 2003; Liu et al., 2013). Since the cracking behavior of A860 and A960 steels varies with the selected H-charging conditions and testing methods, it is not possible to evaluate their susceptibility to HE without further investigations. In all cases, DQ steel with elongated PAGs shows superior resistance to HE in comparison to the equiaxed PAG structures.

For the investigated materials, no correlation is found between H concentration and load/time-to-fracture (Figure 3). DQ has approximately the same H concentration for all the specimens. For A860 and A960, there is a lot more deviation between the results, which might be resulting from varying dislocation densities.

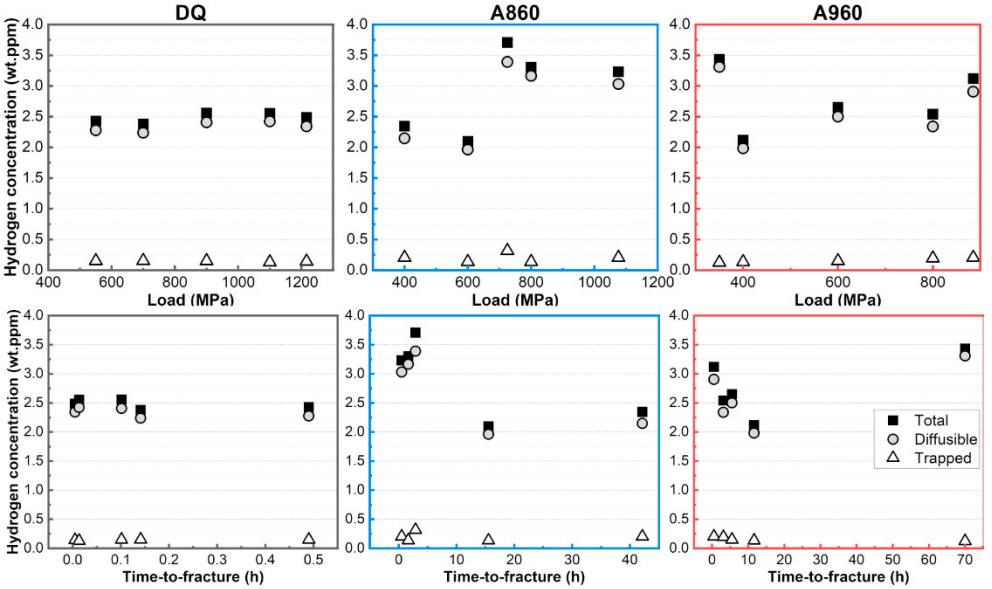

Figure 3. Total, diffusible, and trapped hydrogen concentrations of investigated materials plotted versus load and time-to-fracture.

Fractography of the fracture surfaces shows that DQ has a transgranular quasi-cleavage crack propagation mechanism, and reaustenitized A860 and A960 steels show partly intergranular crack propagation (Figure 4). The grain boundary surfaces of intergranular fracture are not planar and therefore crack propagation can also occur in the vicinity of the grain boundaries. No differences were observed in the cracking mechanisms of A860 and A960 with different loadings at 400 – 800 MPa levels, which further suggests the 800 MPa results to be a deviation.

The crack propagation mechanisms are the same that have been previously observed with TFT (Latypova et al., 2022, 2023b). As cracking behaviors of DQ and A860/960 are repeating under different tests, loads, and H-charging conditions, the quasi-cleavage and intergranular crack propagations are linked to the PAG shapes. The elongated PAG structure is largely irregular in comparison to equiaxed PAGs as presented in Figure 5. When crack propagation occurs transverse to the rolling direction in the elongated PAG structure, the intergranular crack propagation requires a lot more deflections and energy in comparison to the equiaxed PAGs (Nie et al., 2012). Therefore, an elongated PAG structure suppresses intergranular cracking and, in that way, reduces HE susceptibility in comparison to the same alloy steel with an equiaxed recrystallized PAG structure.

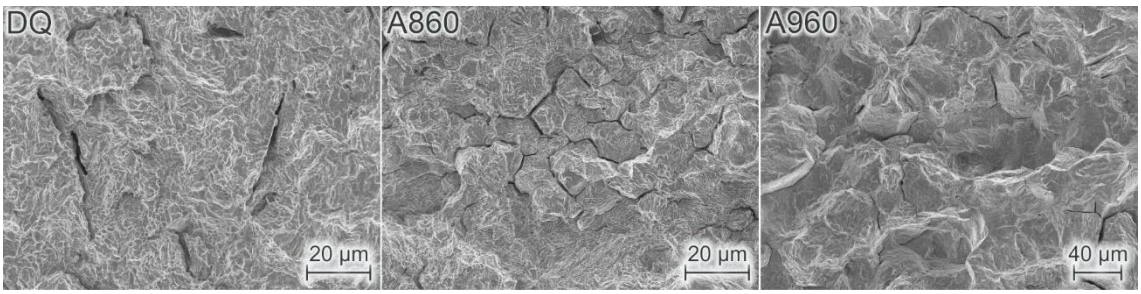

Figure 5. Fracture surfaces of investigated materials.

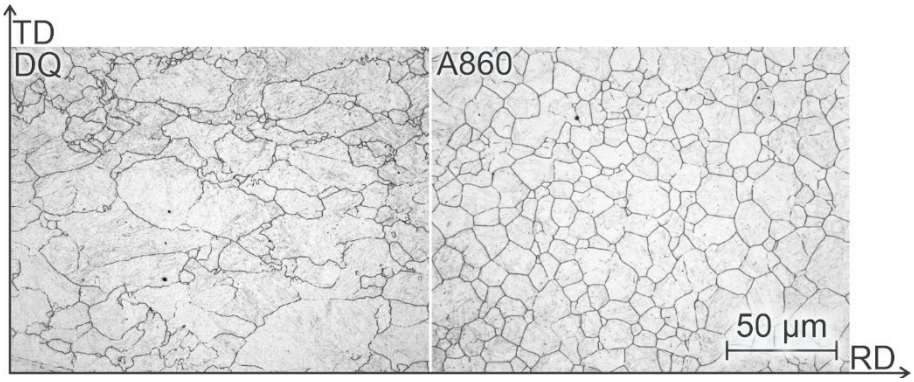

Figure 4. (a) Irregular, elongated PAG structure of DQ and (b) uniform and equiaxed PAG structure of A860.

Figure 6 presents all permeation curves, calculated breakthrough times, and D results. DQ has the slowest D with slightly higher values for A860 and A960. A similar trend was observed in our previous study, where H-charging was conducted using 0.1 M NaOH electrolyte with 1.1 – 1.2 $V_{Hg/HgO}$ cathodic potential, and D was evaluated using a refined successive transient method (Latypova et al., 2023b). For A860 and A960, D is calculated for both the surface and centerline because of differences in dislocation densities, but there is no correlation between D and dislocation density within this dataset. Most likely dislocation density varies among investigated specimens, and it should be measured specifically from each permeation specimen for better correlation.

The main varying parameters that affect D in the investigated materials are PAG grain boundary surface area (S_v) and dislocation density. Grain boundaries have a twofold effect on H diffusion as they can act both as H traps and serve as conduits for rapid H diffusion (Venezuela et al., 2016). S_v increases with finer grain size, which promotes the

mobility of H, but it also leads to a higher density of nodes and triple junctions, which can act as H traps. S_v decreases with increasing grain size, retarding diffusion of H, but it also decreases the trapping effect of nodes and triple junctions, again accelerating H diffusion. The degree of influence of these contradictory effects will change with increasing PAG size, subsequently affecting the H diffusion properties. It has been reported that H diffusion increases for 10 – 46 µm PAG size but after that, the grain coarsening causes a decrease in H diffusivity (Yazdipour et al., 2012). Based on the PAG size of the investigated materials, DQ should have the slowest H diffusion, which speeds up in A860, and even more in A960 steel. Due to grain coarsening, some decrease in D is expected to occur for A960.

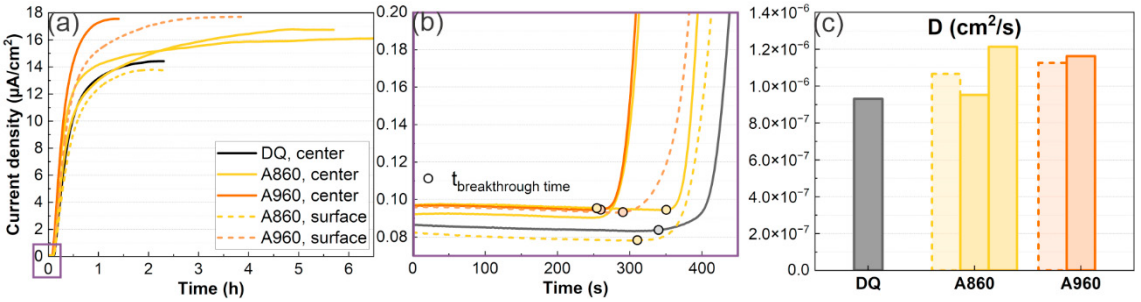

Figure 6. (a) All permeation curves, (b) breakthrough time and (c) calculated diffusion coefficients (D).

Both A860 and A960 have slightly faster diffusion than DQ. However, the difference between A860 and A960 is not statistically significant ($p > 0.05$) (Figure 6c). This suggests that apart from grain coarsening, H diffusion in A960 is slowed down by other microstructural features, and in this case most prominently due to dislocations. Dislocations are reversible traps, and it has been shown that in martensitic AHSS steels, D decreases with increasing dislocation density (Venezuela et al., 2018). Therefore, the relatively small change in D for A960 in comparison to DQ or A860 is most likely the result of two competing effects, a decrease in S_v, which elevates D, and the trapping effect of dislocations, which reduces D. In our previous study, the total H concentration of the materials was measured with TDS after H-charging of the specimens in the same H-charging environment as in this study for 2.5h. Even though no significant differences were observed for the total H concentration of materials, the lower TDS temperature peaks associated with reversible H were higher for A860, and even higher for A960 in comparison to DQ. This further confirms the difference in reversible traps i.e., dislocations (Latypova et al., 2023b), which contributes to retarding of H diffusion in A860 and A960.

In addition to PAG structure and dislocations, there are other grain boundaries, such as lath, block, and packet boundaries that can trap H. In the case of DQ, the last rolling stage is conducted below the recrystallization finish temperature, which produces a high degree of crystallographic discontinuities. These discontinuities can act as potential nucleation sites in fcc-bcc transformation, leading to finer martensitic microstructure and a higher amount of H traps, which further explains the lower D of DQ (Nishioka and Ichikawa, 2012).

4. Conclusions

In-situ constant load tests (CLT) were performed to validate a novel tuning-fork test (TFT) by evaluating the susceptibility of three materials to hydrogen embrittlement (HE). These materials have been previously tested with TFT. The test materials have different PAG shapes/sizes but the same alloying and similar tensile strength and hardness. Additional thermal desorption spectroscopy (TDS) measurements and electrochemical hydrogen permeation (EP) tests were conducted to further investigate the effect of PAG structure on hydrogen trapping and diffusion properties. With both CLT and TFT, direct-quenched DQ steel with an elongated PAG structure has superior HE resistance with longer time-to-fracture and a quasi-cleavage crack propagation mechanism in comparison to equiaxed PAG structures. The effect of equiaxed PAG size on HE susceptibility was inconclusive due to variable results depending on the loading conditions. However, the equiaxed PAG structures always led to partly intergranular crack propagation, which deteriorated HE resistance. Differences between crack propagation mechanisms in elongated and equiaxed PAGs are explained by the geometrical shape of the grain structure. Hydrogen diffusion was slowest for DQ

with a slight increase for equiaxed PAG structures, which was attributed to the simultaneous competing effects of changing grain boundary surface area and higher dislocation density. After CLT, no correlation was observed between hydrogen concentrations and load or time-to-fracture within the materials.

Acknowledgments

We express our gratitude to Business Finland for funding this research. The projects ISA – Intelligent Steel Applications, FOSSA– Fossil-Free Steel Applications, and MASCOT – Materials for CO_2-Neutral Processes in Resource-Intensive Industries are acknowledged.

References

Kimura, Y., Takagi, S., Hara, T., Terasaki, S., Tsuzaki, K., 2003. Hydrogen-induced delayed fracture of a martensitic steel with fine prior-austenite grain size. Journal de Physique IV (Proceedings) 112, 403–406. https://doi.org/10.1051/jp4:2003911

Latypova, R., 2023. The effect of Pd and Ni coatings on hydrogen permeation experiments of as-quenched martensitic steel. Corrosion Reviews 1–8. https://doi.org/10.1515/corrrev-2022-0118

Latypova, R., 2022. Development and application of a novel tuning-fork test in studying hydrogen-induced fracture in as-quenched martensitic steels., Acta Universitatis Ouluensis C 856.

Latypova, R., Nyo, T.T., Kömi, J., Pallaspuro, S., 2023a. Hydrogen embrittlement in as-quenched martensitic steels – application of incremental step loading technique with novel Tuning-fork test. Accepted for publication in Materials Science Forum.

Latypova, R., Nyo, T.T., Seppälä, O., Fangnon, E., Yagodzinskyy, Y., Mehtonen, S., Hänninen, H., Kömi, J., Pallaspuro, S., 2022. Effect of prior austenite grain morphology on hydrogen embrittlement behaviour under plastic straining in as-quenched 500 HBW steels. Procedia Structural Integrity 42, 871–878. https://doi.org/10.1016/j.prostr.2022.12.110

Latypova, R., Seppälä, O., Nyo, T.T., Kauppi, T., Mehtonen, S., Hänninen, H., Kömi, J., Pallaspuro, S., 2023b. Influence of prior austenite grain structure on hydrogen-induced fracture in as-quenched martensitic steels. Engineering Fracture Mechanics 109090. https://doi.org/10.1016/j.engfracmech.2023.109090

Liu, Y., Wang, M., Liu, G., 2013. Hydrogen trapping in high strength martensitic steel after austenitized at different temperatures. International Journal of Hydrogen Energy 38, 14364–14368. https://doi.org/10.1016/j.ijhydene.2013.08.121

Nie, Y., Kimura, Y., Inoue, T., Yin, F., Akiyama, E., Tsuzaki, K., 2012. Hydrogen Embrittlement of a 1500-MPa Tensile Strength Level Steel with an Ultrafine Elongated Grain Structure. Metallurgical and Materials Transactions A 43, 1670–1687. https://doi.org/10.1007/s11661-011-0974-7

Nishioka, K., Ichikawa, K., 2012. Progress in thermomechanical control of steel plates and their commercialization. Science and Technology of Advanced Materials 13, 023001. https://doi.org/10.1088/1468-6996/13/2/023001

Rudomilova, D., Prošek, T., Luckeneder, G., 2018. Techniques for investigation of hydrogen embrittlement of advanced high strength steels. Corrosion Reviews 36, 413–434. https://doi.org/10.1515/corrrev-2017-0106

Standard Practice for Evaluation of Hydrogen Uptake, Permeation, and Transport in Metals by an Electrochemical Technique, 2003. ASTM G148 - 97.

Ungár, T., Ott, S., Sanders, P.G., Borbély, A., Weertman, J.R., 1998. Dislocations, grain size and planar faults in nanostructured copper determined by high resolution X-ray diffraction and a new procedure of peak profile analysis. Acta Materialia 46, 3693–3699. https://doi.org/10.1016/S1359-6454(98)00001-9

Venezuela, J., Liu, Q., Zhang, M., Zhou, Q., Atrens, A., 2016. A review of hydrogen embrittlement of martensitic advanced high-strength steels. Corrosion Reviews 34, 153–186. https://doi.org/10.1515/corrrev-2016-0006

Venezuela, J., Zhou, Q., Liu, Q., Zhang, M., Atrens, A., 2018. Hydrogen Trapping in Some Automotive Martensitic Advanced High-Strength Steels. Advanced Engineering Materials 20, 1700468. https://doi.org/10.1002/adem.201700468

Yazdipour, N., Haq, A.J., Muzaka, K., Pereloma, E. V., 2012. 2D modelling of the effect of grain size on hydrogen diffusion in X70 steel. Computational Materials Science 56, 49–57. https://doi.org/10.1016/j.commatsci.2012.01.003